Microelectronic Engineering 86 (2009) 1676–1679

Contents lists available at ScienceDirect

Microelectronic Engineering

journal homepage: www.elsevier.com/locate/mee

Spectroscopic differentiation between O-atom vacancy and divacancy defects, respectively, in TiO_2 and HfO_2 by X-ray absorption spectroscopy

G. Lucovsky [a,*], K.-B. Chung [a], J.-W. Kim [a], D. Norlund [b]

[a] Dept. of Physics, NC State University, 2401 Stinson Dr., Raleigh, NC 27695-8202, USA
[b] Stanford Synchrotron Radiation Laboratory, Meno Park, CA, USA

ARTICLE INFO

Article history:
Received 3 March 2009
Received in revised form 3 March 2009
Accepted 3 March 2009
Available online 9 March 2009

Keywords:
Monovacancies
Divacancies
X-ray absorption spectroscopy
Pre-edge regime
Bound resonance states
Immobile and mobile vacancies

ABSTRACT

Defect state features have been detected in second derivative O K edge spectra for thin films of nano-crystalline TiO_2 and HfO_2. Based on soft X-ray photoelectron band edge spectra, and the occurrence of occupied band edge 4f states in $Gd(Sc,Ti)O_3$, complementary spectroscopic features have been confirmed in the pre-edge (<530 eV) and vacuum continuum (>545 eV) regimes of O K edge spectra. Qualitatively similar spectral features have been obtained for thin films of HfO_2 and TiO_2, and these have been assigned to defect states associated with vacancies. The two electrons/removed O-atom are not distributed uniformly over the TM atoms defining the vacancy geometry, but instead are localized in *equivalent* d-states: a d^2 state for a Ti monovacancy and a d^4 state for a Hf divacancy. This new model for electronic structure provides an unambiguous way to differentiate between monovacancy and divacancy arrangements, as well as *immobile* (or *fixed*) and *mobile* vacancies.

1. Introduction

This paper addresses the local atom bonding arrangements for intrinsic bonding defects in HfO_2 by extending the range of O K edge X-ray absorption spectroscopy (XAS) measurements into the vacuum continuum regime of X-ray energies and focusing on virtual bound state anti-bonding resonances [1], as well the pre-edge X-ray energies. Most importantly, the spectral results and the assignments to defect state structures confirm a new approach for describing the local electronic structure of vacancy defects that discriminates between mono- and divacancy bonding arrangements based on the multiplicity of defect related spectral features. There has been considerable discussion in intrinsic bonding defects in ZrO_2 and HfO_2 thin films as alternative gate dielectric replacements for SiO_2 and Si oxynitride alloys in advanced Si devices [2]. Conduction band edge traps have been attributed by the Robertson and Shluger groups to O-atom monovacancies, hereafter simply vacancies, as distinct from divacancies [3,4], and by the Lucovsky group to divacancies [5,6]. The former assignments were based on theoretical calculations, whilst the latter were based on the multiplicity of occupied states at the valence band edge as detected by soft X-ray photoelectron spectroscopy (SXPS) [5,6]. These band edge defects are not predicted by calculations in Refs. [3,4], which place the occupied defect states in HfO_2 ands ZrO_2 at, or above mid-gap.

In addition, electron spin resonance (ESR) measurements by the Barklie group indicated an axial symmetry for intrinsic bonding defects in the group IVB elemental oxides, including HfO_2 [7]. The ESR response is consistent with the local bonding geometry of divacancies, and gives additional support to a new paradigm that has introduced for describing the occupied vacancy states. These states are described in the same way as impurity states introduced by first row elements with more d-electrons in their respective atom structures than the two in the group IVB TM atoms.

Equally important, this article combines O K edge XAS measurements in the vacuum continuum regime of X-ray energies, focusing on virtual bound resonance states (VBRS) [1], and on pre-edge O K edge states, each obtained by optimizing data acquisition for extracting second derivative features. These vacuum continuum resonances are enabled by the symmetry of the occupied Hf, Zr and Ti d-states in the vacancy electronic structures. These symmetries introduce non-vanishing matrix elements for transitions between occupied band edge TM atom d-states and final states in which there is an O 1s core hole. The multiplicity of occupied TM d-state features in the VBRS and pre-edge features are consistent with a two electron/removed O-atom description of vacancy sites.

2. Experimental approach and results

Nano-grain HfO_2 and TiO_2 thin films were deposited by remote plasma-assisted CVD onto passivated Si and Ge substrates. Films were annealed in Ar at 700 and 900 °C, resulting in nano-grain

* Corresponding author. Tel.: +1 919 515 73316.
E-mail address: lucovsky@ncsu.edu (G. Lucovsky).

0167-9317/$ - see front matter © 2009 Elsevier B.V. All rights reserved.
doi:10.1016/j.mee.2009.03.005

>3 nm sufficient to support cooperative Jahn–Teller (J–T) degeneracy removal [5,6]. Spectra obtained from samples prepared by reactive evaporation display qualitatively similar spectral features. O K edge spectra indicate significant differences in band edge E_g states consistent with 7-fold coordination in m-HfO_2, and 8-fold coordination in t-HfO_2. Fig. 1 displays second derivative XAS spectra in the O K edge spectral regime at X-ray energies >∼545 eV for m- and t-HfO_2. Fig. 2 displays pre-edge spectra for X-ray energies <∼530 eV for two other HfO_2 films: (i) a 4 nm thick film that displays band edge E_g states that indicate predominantly tetragonal grains, and (ii) a 2 nm thick film in which J–T degeneracy removal is suppressed by a limitation on grain-growth [5,6].

The lowest four features in Fig. 1 are virtual bound anti-bonding d-states resonances with a multiplicity corresponding to the number of occupied d-states in the band edge vacancies. The remaining second seven features are the Hf 5f state features consistent with the crystal field symmetry at the band edge defect states. The transition matrix elements reflect the mixing of Hf 5d and 5f states with O-atom 2p π states into SALCs that are determined by the local symmetry [5,6,8,9]. Different symmetries are clearly evident in Hf 5f features: (i) the spectra for m-HfO_2 do not have a *high symmetry* axis consistent with 7-fold coordination of Hf in m-HfO_2, whereas (ii) the Hf 5f features indicate a 2-fold symmetry axis, but with distortion of the features at lower, and higher X-ray energies. These distortions result from a cooperative J–T distortion in tetragonal HfO_2 in which Hf 5d-state degeneracies are removed by basal planes distortions, resulting in symmetry changes and in-equivalence of *side-band features*. The differences in the spectra in Fig. 2 indicate two doublet features with a factor of 1.4 difference in splitting. These are consistent with two types of vacancies [10]: (i) immobile divacancies that are encapsulated with a distorted octahedral environment characteristic of a distorted CaF_2 lattice, and (ii) mobile vacancies that are either on the surface of nano-grains, or on internal grain boundaries, and are encapsulated with fewer than six Hf atoms.

Fig. 3 presents the pre-edge spectra for nano-grain TiO_2. These spectra indicate two doublet features that are also consistent with two types of monovacancies: (i) immobile vacancies that are completely encapsulated by three Ti atoms within a distorted rutile or anatase lattice; and (ii) mobile vacancies that are encapsulated with fewer than three atoms either on surfaces, or internal grain boundaries. The ratio of splittings in this case is larger two than for HfO_2, consistent with the lower coordination at the monovacancy site, three compared to six for HfO_2.

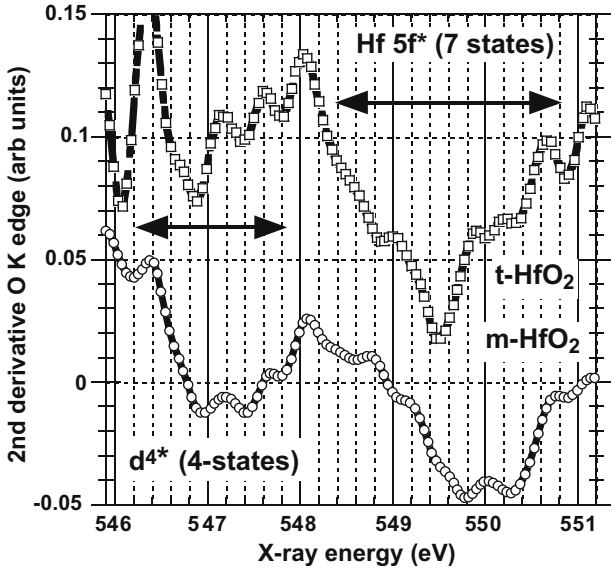

Fig. 1. Virtual bound resonances in vacuum continuum region of O K edge second derivative XAS spectra for thin film m- and t-HfO_2.

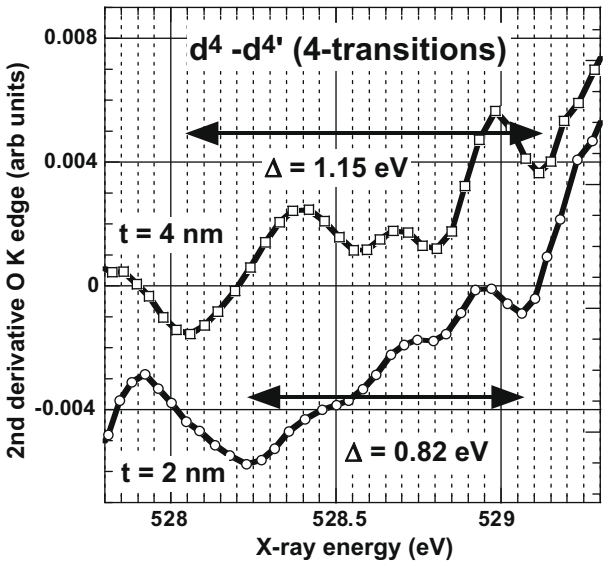

Fig. 2. Highest 5d–5d′ transitions for divacancy d^4 defects in the pre-edge second derivative XAS O K edge spectra for 4 nm thick and 2 nm thick HfO_2 thin films.

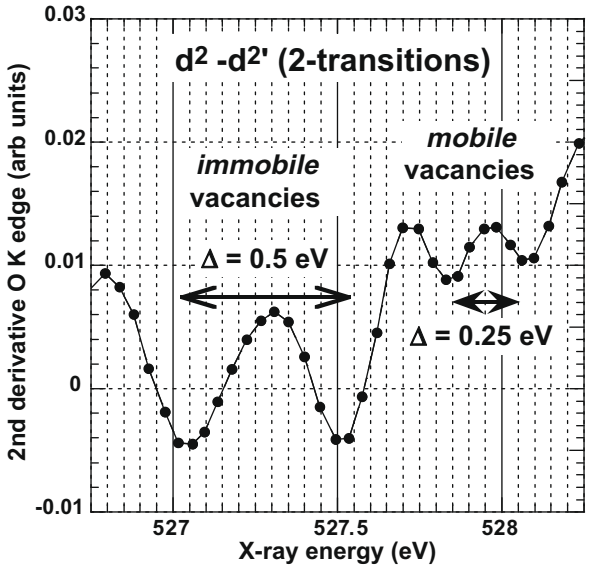

Fig. 3. Pre-edge O K edge second derivative XAS spectra for fixed and mobile vacancies in thin film TiO_2.

3. Discussion: occupied band edge states in $GdScO_3$ and $Gd(Sc_{0.96}Ti_{0.04})O_3$

Fig. 4 compares differentiated valence band spectral features for $GdScO_3$ and $Gd(Sc_{0.96}Ti_{0.04})O_3$, high-lighting the valence band edge features at energies above the highest occupied valence band O-atom 2p π non-bonding states. The second derivative spectral trace for $GdScO_3$ indicates seven Gd^{3+} 4f band edge occupied features corresponding to the half-filled 4f states. Two additional features are found in the corresponding spectral trace for the $Gd(Sc_{0.96}Ti_{0.04})O_3$ alloy. These are attributed to the Ti^{3+} band edge 3d occupied states of the substituted Ti. The Ti^{3+} and Sc^{3+} ions are on

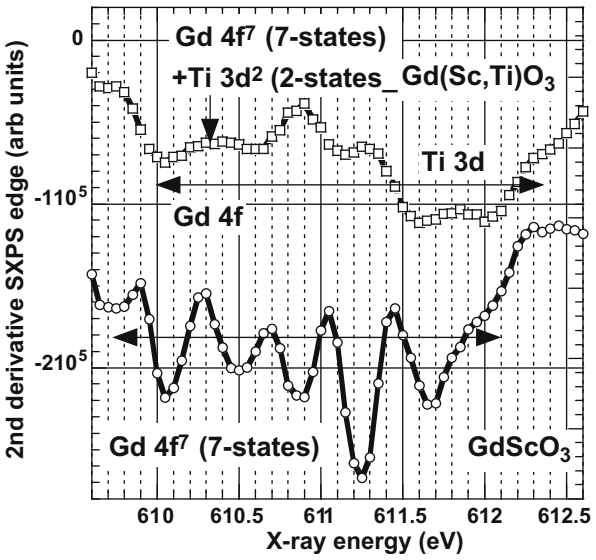

Fig. 4. Band edge Gd 4f and Ti 3d features in pre-edge SPXS spectra for $GdScO_3$ and $Gd(Sc_{0.96}Ti_{0.04})O_3$.

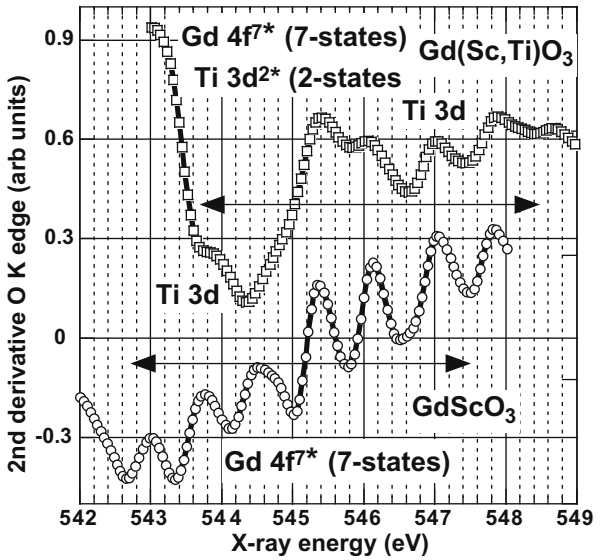

Fig. 5. Gd 4f and Ti 3d anti-bonding features in vacuum continuum region of O K edge second derivative XAS spectra for $GdScO_3$ and $Gd(Sc_{0.96}Ti_{0.04})O_3$.

separate bonding sites, and with Ti atoms incorporated at random, and the Gd 4f and Ti 3d spectral features are superposed.

Fig. 5 compares the lowest the lowest energy lowest energy bound virtual resonance states. These features are assigned to symmetry induced states associated with a hole on the occupied state spectra features in Fig. 4. This interpretation is also supported by the *mirrored asymmetry* into groups of three and four spin-orbit split states in the corresponding valence band edge and virtual bound state regimes. The same three triplet Gd 4f states observed in the optical absorption spectrum as discussed in Refs. [11,12] are also found in pre-edge XAS spectra.

4. Conclusions: interpretation of pre-edge and VBRS spectral features

In Refs [5,6], it was noted that d-state occupied and empty features detected spectroscopically at valence and conduction band

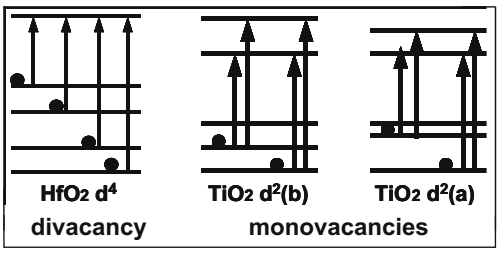

Fig. 6. Energy level diagrams proposed for d–d′ transitions associated with monovacancy and divacancy d^2 and d^4 defects in nano-grain TiO_2 and HfO_2, respectively.

edges in HfO_2 and ZrO_2 could not be explained by the calculations in Refs [3,4], but were consistent with bonding that expected from tri-valent, rather than tetra-valent bonding at the defect sites [7,13]. This approach is reinforced by the spectral features observed for TiO_2, and the SALC of Ti- and O-atom molecular orbital states for the trivalent Ti ion cluster, $Ti(HOH)_6^{3+}$ [14].

The multiplicity of features in the VBRS spectra are equal to two electrons/O-atom removed. We propose that these result from occupied band edge TM atom states with d^2 and d^4 occupancies in HfO_2, and TiO_2, respectively. Based on soft X-ray photoelectron band edge spectra and the occurrence of occupied band edge 4f states in $GdScO_3$, complementary spectroscopic features are present in the pre-edge (<530 eV) and vacuum continuum (>545 eV) regimes of O K edge spectra. Qualitatively similar spectral features have been obtained for thin films of HfO_2 and TiO_2 and these were addressed in Section 2. In analyzing the O K edge spectra in the pre-edge and vacuum continuum regimes, it was assumed that the two electrons/removed O-atom are not distributed over the TM atoms that were previously bonded to that atom as in Refs. [3,4], but instead were localized in *equivalent* d-state orbitals with occupancies consistent with either a mono- or divacancy structure. This approach results in a d^2 state for a Ti vacancy and a d^4 state for a Hf divacancy. These localized *equivalent* d-states: a d^2 state for a Ti vacancy and a d^4 state for a Hf divacancy then provide a basis for the interpretation of spectral results in a way that parallels the features associated with the occupied Gd 4f and Ti 3d features in the corresponding spectra for the $Gd(Sc,Ti)O_3$ alloy discussed in Section 2.

The defect related features in derivative O K edge spectra are quantitatively different, four for the Hf 5d-states, and two for the Ti 3d-states, and consistent with the number of features associated with the electronic structures the respective *equivalent* d-states used to model the vacancy electronic structures: a d^2 state for the Ti vacancy and a d^4 state for the Hf divacancy. This provides an unambiguous basis for differentiating between vacancy and divacancy arrangements. Finally, Fig. 6 presents energy level diagrams proposed for d-state occupancy and d–d′ transitions for vacancy and divacancy defects in the d^0 group IVB elemental oxides, TiO_2 and HfO_2, respectively. Finally, differences in the width of the transition state features in the pre-edge spectra for >3.5 nm thick-nm-/*t*-HfO_2 films with J–T splittings, and thinner HfO_2 films <2 nm thick, in which grain-growth is dimensionally suppressed, provide a spectroscopic approach to discriminating between immobile fully coordinated divacancies within nano-grains, and mobile under coordinated divacancies, either on grain surfaces, and internal grain boundaries.

References

[1] R.M. White, T.H. Geballe, Long Range Order in Solids, Solid State Physics Supplement, vol. 15, Academic Press, New York, 1979 (Chapter IV).
[2] M. Houssa, M.M. Hyens, in: M. Houssa (Ed.), High-K Gate Dielectrics, Institute of Physics, Bristol, 2004 (Chapter 1.1).

[3] K. Xiong, J. Robertson, M.G. Gibson, S.J. Clark, Appl. Phys. Lett. 87 (2005) 183505.
[4] J.L. Gavartin, D.M. Munoz-Ramo, A.L. Shluger, G. Bersuker, B.H. Le, Appl. Phys. Lett. 89 (2006) 082908.
[5] G. Lucovsky, H. Seo, S. Lee, et al., Jpn. J. Appl. Phys. 46 (2007) 1899.
[6] G. Lucovsky, J. Mol. Struct. 838 (2007) 187.
[7] S. Wright, S. Feeney, R.C. Barklie, Microelectron. Eng. 84 (2007) 2378.
[8] F.A. Cotton, Chemical Applications of Group Theory, second ed., Wiley Interscience, New York, 1963 (Chapter 8).
[9] P.A. Cox, Transition Metal Oxides, Clarendon, Oxford, 1992 (Chapters 2, 3 and 5).
[10] S. Guha, V. Narayanan, Phys. Rev. Lett. 98 (2007) 196101.
[11] S.-G. Lim, S. Kriventsov, T.N. Jackson, et al., J. Appl. Phys. 91 (2002) 4500.
[12] D.S. McClure, Electronic Spectra of Molecules and Ions in Crystals, Academic Press, New York, 1959.
[13] S. Wright, R.C. Barklie, J. Mater. Sci.: Mater. Electron. 18 (2007) 743.
[14] H.B. Gray, Electrons and Chemical Bonding, Benjamin, New York, 1965 (Chapter IX).